Title

CO_2 plume migration in underground CO_2 storage: the effects of induced hydraulic gradients

Authors

H. Vosper[a*], R. A. Chadwick[a], G. A. Williams[b]

[a]British Geological Survey, Nicker Hill, Keyworth, NG12 5GG

[b]British Geological Survey, Research Avenue South, Edinburgh, EH14 4AP

[*]hayleyv@bgs.ac.uk

Abstract

The use of water production as a pressure mitigation tool in the context of CO_2 storage is widely studied but the impact it might have on the migration behaviour of a buoyant CO_2 plume is less well reported. To investigate this further two different scenarios were modelled. In the first, a single water production well was used to draw CO_2 along the strike of an open aquifer with a regional dip. Large rates of water production (5 - 10 times the volume of injected CO_2) were required to achieve only small displacements of the CO_2 plume. The second scenario investigated to what extent an induced hydraulic gradient might spill CO_2 already stored in a structural trap. Here the effects were more pronounced with over 90% of the CO_2 being spilled at a water cycling rate of 10 Mt per year (corresponding to a hydraulic gradient of 1.28 bar/km). The modelling was tested by the real case at Sleipner where CO_2 migration in the Utsira Sand is potentially impacted by water production at the nearby Volve field. Simulations concluded that the CO_2 plume at Sleipner should not be materially affected by water production from Volve and this is supported by the time-lapse seismics.

Keywords

CO_2 storage; water production; plume steering; Sleipner; Utsira Sand.

1. Introduction

It is widely recognised that global CO_2 emissions must be drastically reduced to limit the detrimental impact of climate change. One of the main strategies for this is to capture CO_2 at source and store it in deep geological reservoirs. In the context of underground CO_2 storage, water production from wells is cited as a technique for controlling and mitigating the increase in reservoir pressure that might arise from injecting large volumes of CO_2 (Breunig et al., 2013; Buscheck et al., 2012). A secondary application of water production might be to influence the position and/or the migration trajectory of the injected CO_2 plume. So plume steering might be used to prevent the buoyant plume from approaching areas identified as higher risk, such as permeable faults, vulnerable wellbores, areas with less suitable caprock, or even adjacent subsurface operations. Plume steering might also be used to increase the length of the CO_2 migration pathway to increase dissolution and capillary trapping, both of which act to stabilise the CO_2 plume by reducing its mobility and buoyancy, and render the storage less reliant on the caprock as a barrier to leakage.

Pressure management by water production during CO_2 injection is mainly to counter induced geomechanical instability, and has been the subject of numerous modelling studies: limiting local pressure increase (Bergmo et al., 2011; Buscheck et al., 2012); reducing the increased pressure spatial footprint (Buscheck et al., 2011; Court et al., 2012); providing an intervention when site pressure exceeds design limits (Le Guenan and Rohmer, 2011); or targeting a specific area which might be vulnerable to increased pressure (Birkholzer et al., 2012). Multiple modelling studies consider the well positioning, well numbers and well production rates required to optimally control pressure increase and maximise CO_2 injectivity and reservoir storage capacity. Pressure reduction is most effective in reservoirs with high permeability, weak permeability heterogeneity and with water production close to the CO_2 injection (Birkholzer et al., 2012; Chadwick et al., 2009; Cihan et al., 2015).

Several of these modelling studies cite plume displacement as a possible consequence of pressure management but few studies explore this in greater detail. Buscheck et al. (2012) investigated whether the buoyancy forces which drive CO_2 migration up-dip could be overcome by down-dip water production. The authors found that in a 2D model with a 5.7° slope, producing a volume of water equivalent to that of the injected CO_2, from 10 km down-dip of the CO_2 injection point, was sufficient to prevent CO_2 travelling up-dip, with breakthrough at the production well not occurring for 20-50 years depending on the permeability. Court et al. (2012) simulated CO_2 injection with water production via a 5-spot pattern with four production wells surrounding an injection well. Very little impact on plume position or thickness was found, even on a 50-year timescale, probably because the production wells were tending to pull the CO_2 in mutually cancelling directions.

Cameron and Durlofsky (2012) investigated means of maximising residual and dissolution trapping. They produced water from the deepest parts of the reservoir, well away from the CO_2, and reinjected it directly into accumulations of CO_2, vertically above the injection wells. Their strategy was to use periodic water cycling in discrete events optimized for the trapping of CO_2, but the practicalities of injecting water directly into over-pressured CO_2 were not discussed. Similarly, Leonenko and Keith (2008) explored the dissolution potential of water injection. They used the same well for both CO_2 injection and subsequent water reinjection at the top of the reservoir, with water production further afield. Dissolution was enhanced by the water cycling as the plume was forced away from the injection well and into contact with more CO_2-free water in the surrounding reservoir.

The potential impact of water production on plume position has yet to be assessed for a range of reservoir types. The main aim of this paper is to investigate the effectiveness of water production as a tool to manipulate the migration trajectory of free CO_2 in storage reservoirs and to quantify the volumes required to have a noticeable impact on plume position. Three numerical fluid flow models are used to examine plume steering in different settings. Firstly a simple box model with a regional dip is used to investigate to what extent water production can perturb a plume of CO_2 away from its buoyancy-driven up-dip pathway. This is relevant to the early stages of a CO_2 storage operation or to storage in an open aquifer. The second model incorporates structural trapping within a small domal feature to quantify the amount of water production (and the resulting hydraulic pressure gradient) that is required to draw CO_2 out of a structural closure. The parameters for both models are based around the Sleipner storage operation, and a third model is used to test the sensitivity of observed plume migration at Sleipner to water production at the Volve Field only 8 km away.

2. Planar topseal with a regional dip

A simple box model was chosen to examine the influence of water production in the absence of complexities such topseal relief or reservoir heterogeneity. A flat horizon representing an impermeable topseal defines the top of the model, which is then tilted slightly to give a regional dip to the south; the deepest part of the reservoir is at the southern boundary.

2.1. Model description and parameters

The box model extends 7.5 km each way along the strike from the injection well, 7.5 km down-dip (south) and 22.5 km up-dip (where CO_2 is expected to migrate). The thickness of the reservoir is 200 m, bounded above and below by impermeable boundaries. Pore-volume multipliers with a value of 10^6 are used on the outer lateral edges of the model to provide approximately hydrostatic boundary conditions, equivalent to a very large uncompartmentalised aquifer. The total pore-volume in the model is 2.4×10^8 km^3, easily sufficient to contain realistic quantities of CO_2. This 'open aquifer' configuration prevents boundary effects which might otherwise complicate results.

The top of the model centre is placed at a depth of 1000 m below sea level, beneath the impermeable topseal boundary and a regional dip of 0.5 degrees to the south is applied, similar to average dips at the top of the Utsira Sand at Sleipner (Chadwick and Noy 2010).

A uniform grid is used with a lateral cell size of 100 m and with the 200 m thick reservoir divided into 26 layers, increasing from 0.7 m thick at the top to 20 m at the base. All simulations are run using the Schlumberger ECLIPSE black-oil simulator.

Model parameters chosen for this study (Table 1, Figure 1) roughly reflect storage conditions in the Utsira Sand at Sleipner and follow Noy et al. (2012). Average reservoir temperature is taken from Chadwick et al. (2012) and initial pressure is set to hydrostatic.

Parameter	Value
Porosity	0.37
Permeability	3040 mD
Permeability anisotropy Kv/Kh	1
Rock compressibility	4.5 x 10-5 bar-1
Temperature	35 °C
Salinity	32, 000 ppm
CO_2 injection rate	1 Mt/year

Table 1: Parameter values for the base-case

A single injection well is positioned centrally along strike in the model, perforated in the deepest cell, with a CO_2 injection rate of 1 Mt/year for a period of 15 years. A single production well positioned 5 km to the northwest of the injection well, perforated in the deepest cell only, is used to simulate water extraction from the reservoir for 16 years (one year longer than the injection period). This location, diagonally up-dip of the injection point, is chosen to have a cross-slope influence on the CO_2 plume throughout the production period.

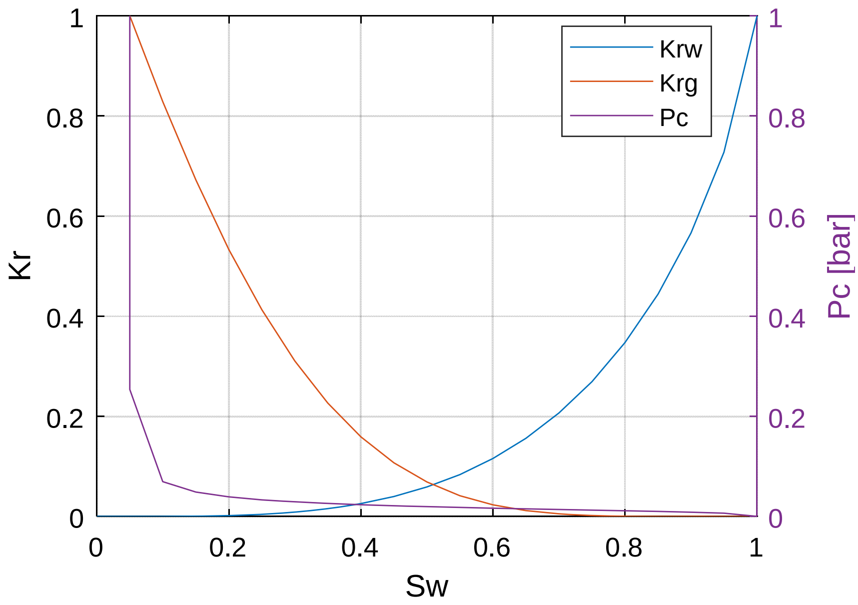

Figure 1: Relative permeability and capillary pressure data used for all simulations, based on the Utsira Sand, taken from Noy et al. (2012).

The rate of water extraction is fixed as a multiple of the volume of CO_2 injected. The volumetric injection rate, assuming a CO_2 density under the ambient reservoir conditions of 717 kg/m^3 (NIST, 2016), was 1.39 x 10^6 rm^3/year, so the equivalent mass of water to be extracted is 1.43 Mt/year (assuming a water density of 1022 kg/m^3). This approach of measuring produced water in terms of injected CO_2 volumes is widely used (Birkholzer et al., 2012; Buscheck et al., 2012; Court, 2011).

2.2. Plume migration with the base-case flow model

A base-case model without any water production was run first, to simulate the purely buoyancy-driven flow of injected CO_2 (Figure 2). Initially the CO_2 rises to the top of the model, reaching the topseal after 3 months. The plume then spreads as a thin layer beneath the topseal, initially almost radially but soon with a marked bias up-dip towards the north, consistent with analytical approximations of buoyant flow beneath a sloping caprock (Vella and Huppert, 2006). After the end of injection the CO_2 plume continues to migrate northwards as a thin layer (~20 m thick), leaving behind a trail of residually trapped CO_2. Residually-trapped CO_2 saturations do not fall below 0.2 since the CO_2 becomes immobile in accordance with the relative permeability curves. The simulation indicates that, post-injection, the up-dip velocity of the plume stabilises to 0.10 km/year with an R-squared value of 0.999. For comparison, the Vella and Huppert (2006) analytical solution gives an up-dip plume velocity in the post-injection phase of 0.11 km/year. Slight discrepancies between the analytical and numerical solutions can be accounted for by factors such as capillary trapping and dissolution. Pressure increase due to CO_2 injection is less than 0.5 bar in any given grid cell, giving no concern with regard to fracture pressure.

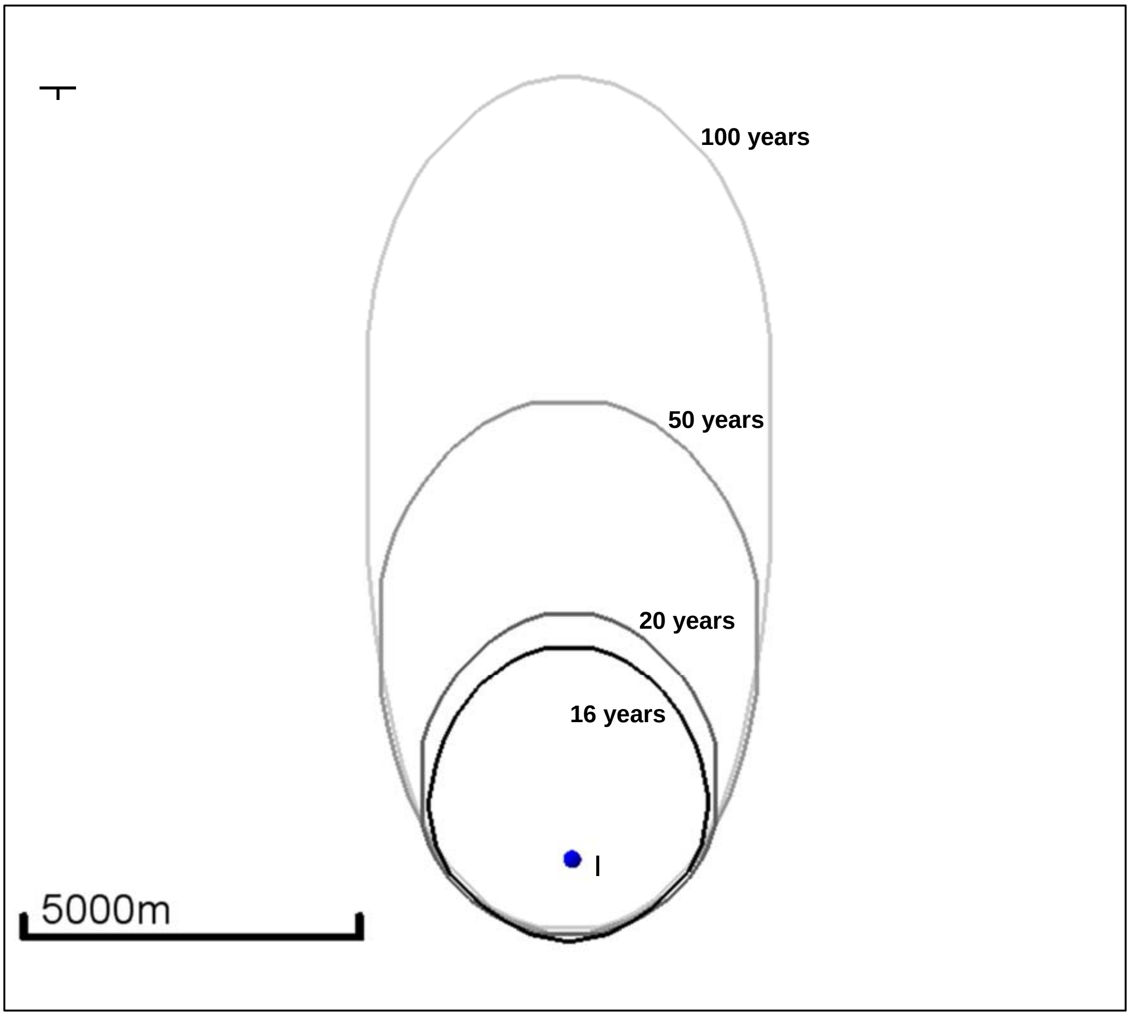

Figure 2: Base-case plume extents at labelled time steps (after start of injection). CO_2 injection well marked as I. Dip marker indicates the reservoir dip to the south.

2.3. Plume deviation with varying rates of water production

A series of simulations was then run with increasing amounts of water production, set as multiples (0, 1, 2, 5 and 10) of the reservoir volume of injected CO_2 (Figure 3). For the first 20 years of simulation there is very little impact on the position of the CO_2 plume for volumes of produced water up to twice the amount of injected CO_2. Effects on plume spreading only become significant for extracted amounts of water 5 or 10 times the volume of injected CO_2. The impact of water extraction is most marked at the end of the production period (16 years), with the northwest flank of the plume displaced by more than a kilometre at higher rates of water production. Subsequent to the cessation of water production, buoyancy takes over as the principal plume driving force and the longer-term effect of water production on CO_2 migration is minimal.

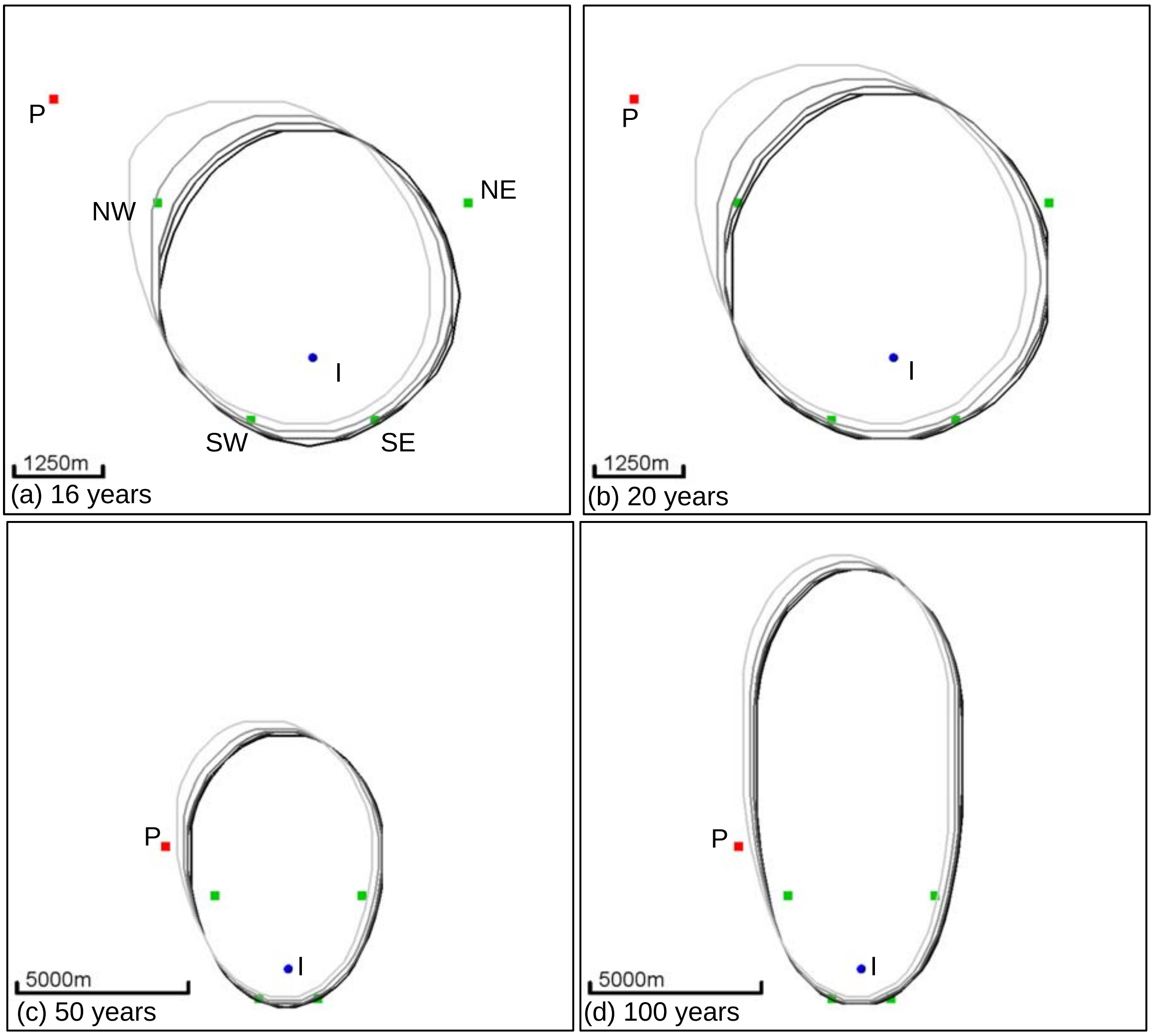

Figure 3: Plume extents for a range of production volumes (dark grey to light): 0:1 (base-case), 1:1, 2:1, 5:1 and 10:1. Water production well P, sampling points (Figure 4) green. Note change of scale on later plots.

2.3.1. Fluid saturation changes

In order to compare changes in CO_2 saturation associated with the scenarios, four 'sampling' locations were chosen to measure gas saturations around the injection well (Figure 3a). The sampling points to the SW and SE of the injection well are 1.2 km away, and those to the NW and NE are 3 km away, the former being closer to the injection point to ensure the presence of CO_2 to measure.

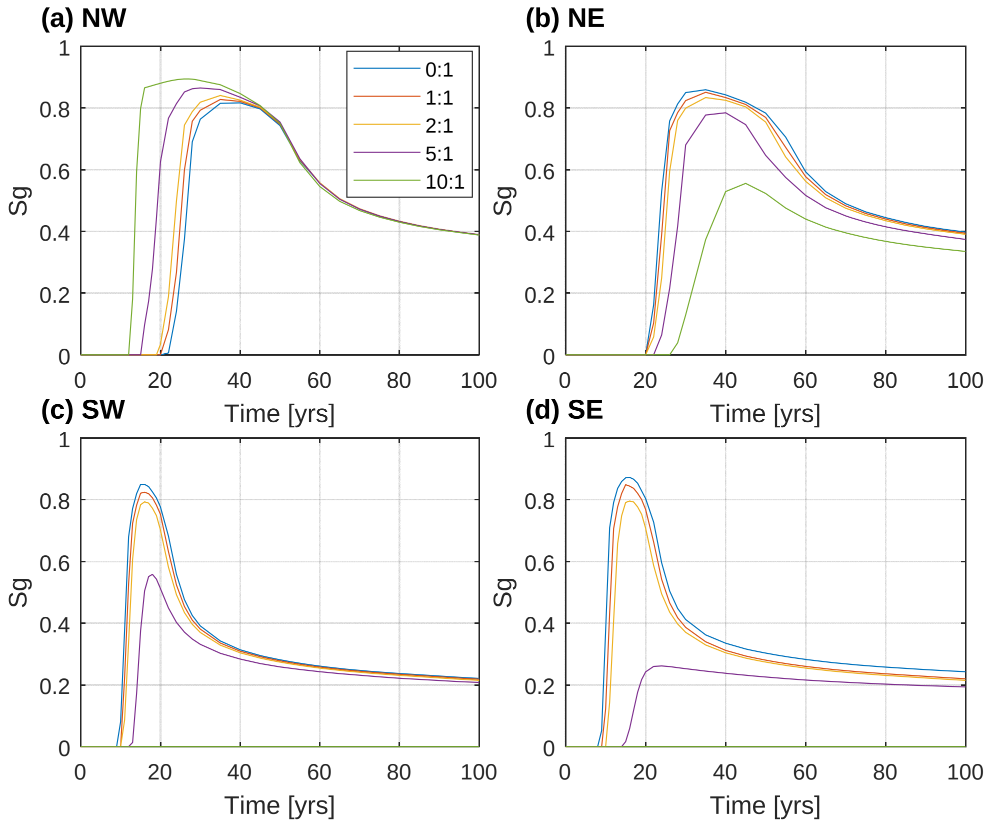

Figure 4: Gas saturation in the top cell of the reservoir at the sampling points (for locations see Figure 3).

The larger the water production rate, the greater the impact on the CO_2 plume. The arrival time of CO_2 at the NW sampling point (located in the direction of the production well) becomes progressively earlier as larger amounts of water are produced. So without water production, CO_2 arrives after 22 years, whereas with a 10:1 production ratio arrival occurs after only 12 (Figure 4a). At the NW sampling point CO_2 saturations are always higher for the larger water production ratios. For the remaining sampling points, NE, SE and SW of the injection well, increased water production progressively delays arrival of the CO_2, and reduces saturations, to the extent that the 10:1 production ratio completely prevents CO_2 arriving at the SW and SE sample points (Figure 4c, d). This demonstrates that water production can steer a plume of CO_2 away from specific localities, but the relative amount of perturbation at the scale of the full plume is quite small (Figure 3). It is noted that no CO_2 reached the production well in any of these simulations, either in free or dissolved form.

2.3.2. Pressure changes

The area of low pressure created by water production dissipates radially with distance from the production well and is superimposed on the pressure increase created by CO_2 injection (Figure 5). For the first 15 years of the simulation both injection and production wells are operational, and each creates its own local pressure perturbation. Water production continues for one year beyond cessation of injection, and the pressure in the reservoir significantly decreases. After the end of production (16 years) the pressure moves rapidly towards equilibrium because of the high reservoir permeability and open model boundaries.

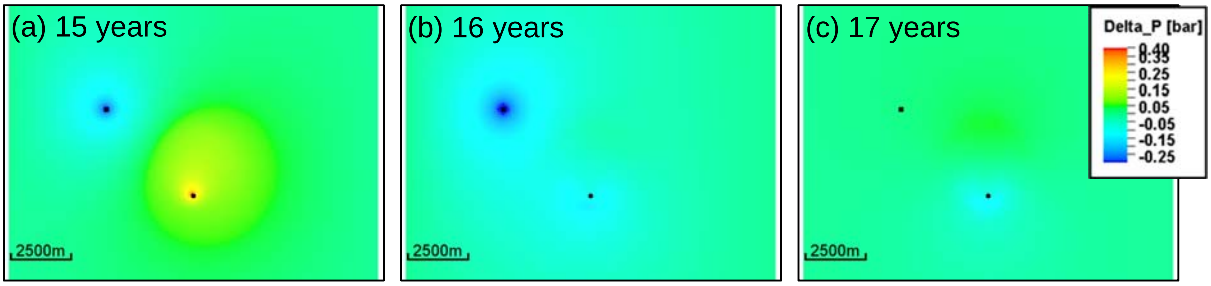

Figure 5: Pressure change (relative to hydrostatic) created by injecting and producing equal volumes of CO_2 and water respectively at time steps (a) 15 years i.e. end of injection, (b) 16 years i.e. end of production and (c) 17 years.

An additional simulation case was run where water was extracted from the entire reservoir interval, rather than from just the deepest cell. There was no discernible difference in the location of the CO_2 plume or the hydraulic gradient at the plume. This is because of the large lateral extent of the model reservoir compared to its thickness.

2.4. Plume deviation with a modified production well position

In the base-case simulation the water production well was located 5 km away from the injection point and no CO_2 (free or dissolved) was produced. If the water extraction well were moved closer to the injection point a larger influence on CO_2 migration would be expected, but at a greater risk of CO_2 breakthrough. In order to test this trade-off an additional model was run with the production well positioned 3 km from the injection point (Figure 6).

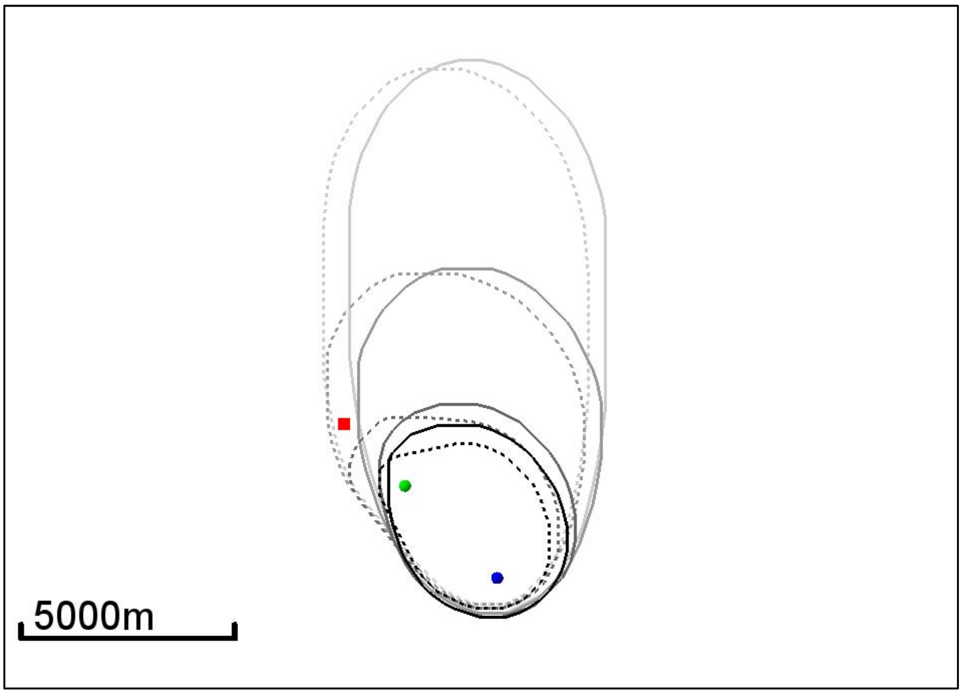

Figure 6: A comparison of the plume extent at time steps 16, 20, 50 and 100 years (dark to light) between cases with the production well located 5 km (solid lines, red square) and 3 km (dashed lines, green circle) away from the injection point (blue circle). The extraction ratio is 10:1.

The additional effectiveness of producing water from the nearer location is shown by the long-term migration path which is displaced a further 500 m to the west. However a consequence of this is that the plume quickly intersected the producing well at 3 km, resulting in the production of CO_2 through the well from about 8 years onwards (Figure 7). The total amount of CO_2 produced from the base cell of the reservoir was 93 kt, 0.6% of the total injected amount. This production of CO_2 undermines the purpose of the CO_2 storage operation. An additional simulation was run where water was extracted over the entire reservoir interval, 3 km from the injection well. In this scenario over 1 Mt of CO_2 was produced (Figure 7). This accounts for 7% of the total injected amount, and highlights the strong benefits of producing water from only the base of the reservoir when there is any risk of the plume reaching the extraction well.

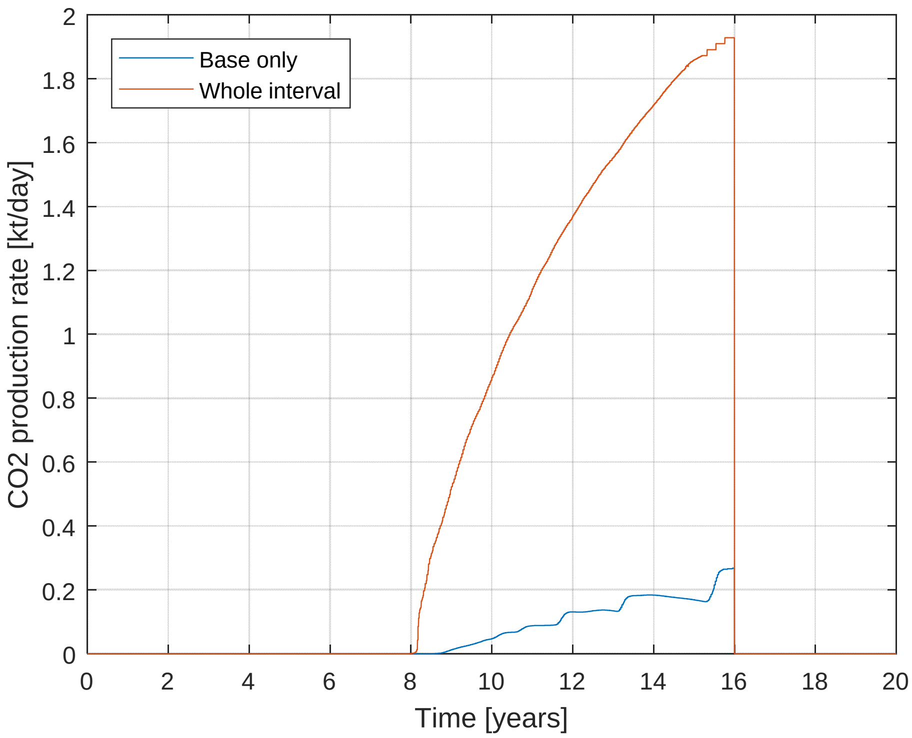

Figure 7: Total production rate of CO_2 (free and dissolved) from the production well located 3 km from the injector. Production continues for 16 years.

It is clear therefore that optimising the trade-off between obtaining maximum plume steering and preventing premature CO_2 breakthrough is not trivial.

2.5. Plume deviation with a different well position relative to the dip

A second set of simulations was run with the production well positioned to the SW of the injection point, diagonally down-dip. By the end of the water production stage there is a drawing of the plume by 1 km SW towards the production well for higher production ratios, as noted previously for the NW production well. This enhanced spread of the plume to the SW of the injection well is maintained over the longer term, because of residual saturations of CO_2 becoming fixed due to capillary trapping.

2.6. Plume deviation with reduced reservoir permeability

To investigate the sensitivity of plume movement to reservoir permeability, two additional scenarios are examined, with permeability reduced to 1000 and 500 mD and the extraction ratio fixed at 10:1 (Figure 8). Halving the permeability roughly doubles the time it takes for the plume to migrate a given distance (Figure 8b, c). In consequence, with reduced reservoir permeability, even large amounts of water production have very little impact on plume migration when production is limited to 16 years (Figure 8b, c). Although the pressure differences are greater when the permeability is reduced, the low permeability reduces the speed at which CO_2 is able to migrate towards the production well. So permeability is a limiting factor on the effectiveness of water production as a tool to influence the migration pathway. Longer times are required for CO_2 to migrate a given distance in a low permeability reservoir (Figure 8) and it follows that to achieve the same migration of CO_2 towards a production well the duration of water production would need to be increased.

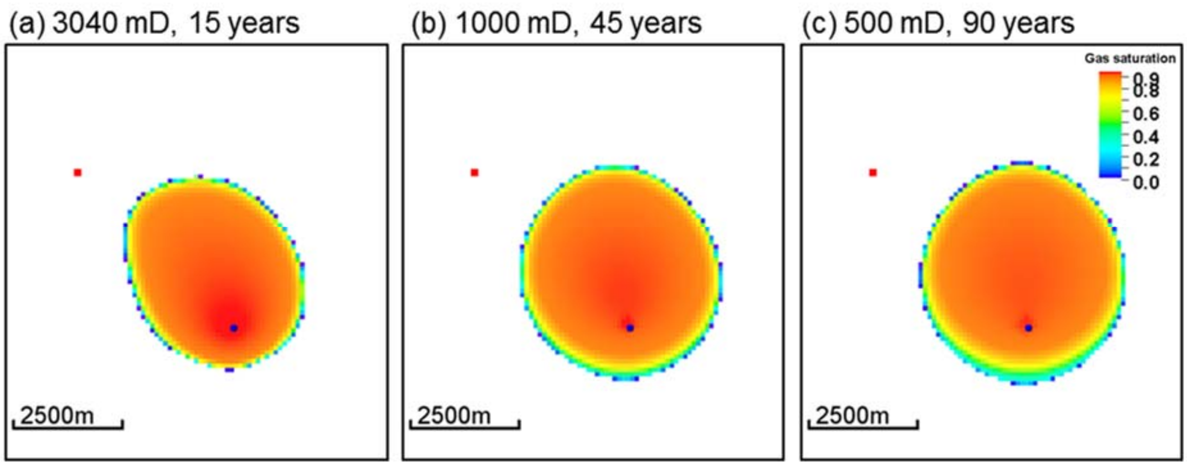

Figure 8: CO_2 saturation in the top layer of the model with a 10:1 ratio by volume of water production and CO_2 injection. Injection wells are marked with blue circles and production wells are marked with red squares (5 km apart). Water is produced for 16 years in all cases.

2.7. Plume deviation with reduced vertical permeability

Permeability anisotropy is common in geological reservoirs, with horizontal fabrics of less permeable material such as silt and shale restricting vertical permeability. To test the impact of permeability anisotropy the vertical permeability was reduced by a factor of 10 to 304 mD. This resulted in a longer time for the plume to reach the top of the reservoir; more than 2 years compared with the 5 months it took with isotropic permeability. In addition, the water production has a smaller effect on the plume location for the reduced vertical permeability case because the CO_2 was unable to travel as far in the given 16 year production time period.

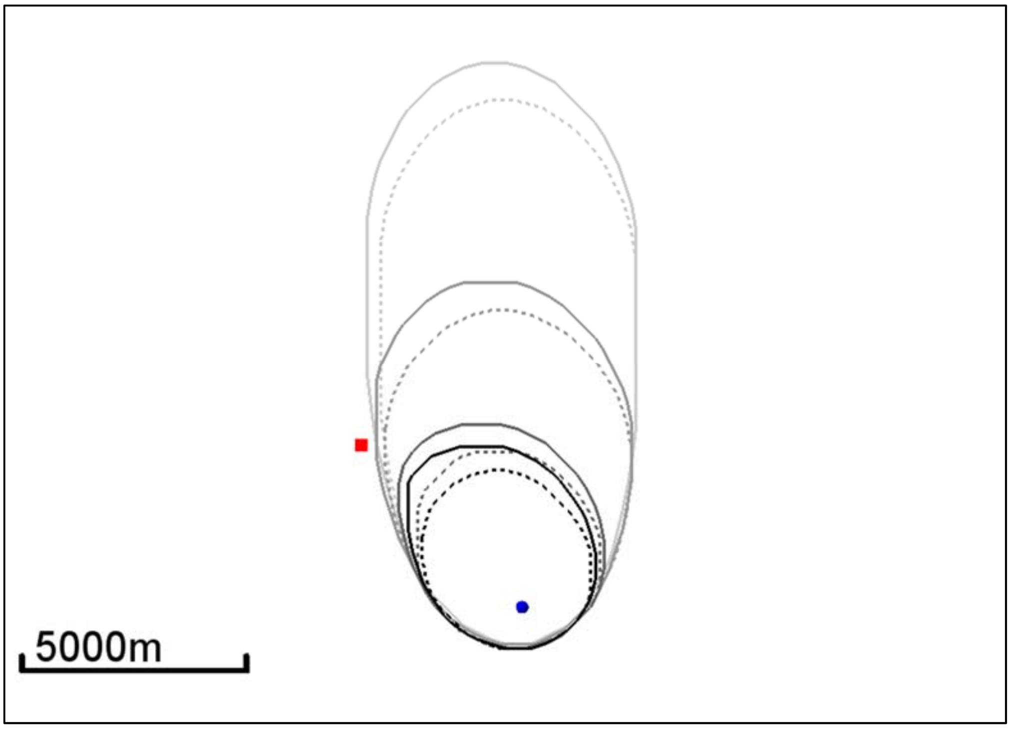

Figure 9: Comparison of the plume extent with permeability anisotropy Kv/Kh=1 (solid lines) and Kv/Kh=0.1 (dashed lines). The water extraction ratio is 10:1, and displayed time steps are 16, 20, 50 and 100 years (dark to light).

2.8. Summary

During the water production phase, a noticeable influence on the position of the CO_2 plume is observed if the volume of water produced significantly exceeds the volume of CO_2 injected (only by factors of 5x and above). After water production ceases, which for practical reasons is likely to be roughly when injection ceases, the CO_2 reverts to primarily gravity-driven migration and is free to continue travelling up-dip, subject to residual trapping and dissolution. Overall on a 100 year time-scale, the hydraulic gradient caused by producing water up to 10 times the volume of CO_2 injected has very little impact on the plume position. In this open aquifer configuration, and particularly with lower permeability reservoirs, water production is not generally effective as a plume steering tool. There might be an exception if the induced hydraulic gradient forces the plume past a spill-point or other topographical feature which would change the natural path of the plume.

3. Structural trapping with an induced hydraulic gradient

Buoyant migration of CO_2 beneath a smoothly dipping topseal in a homogeneous reservoir without a hydraulic gradient is uniformly up-dip with immobilisation of the CO_2 depending entirely on capillary trapping and/or dissolution. Lateral migration or ‘wandering’ of the CO_2 plume, either natural or induced, can have both positive and negative trapping impacts.

On the positive side, topographic ‘roughness’ on the topseal surface will tend to increase storage capacity as CO_2 becomes buoyantly trapped in local domal features. Migration meandering produced by topseal topographic relief or by reservoir heterogeneity will increase the length of migration pathways and enhance the effect of stabilising processes. On the negative side, plume wandering would increase its spatial footprint, increasing the potential for reaching leakage pathways and also increasing the spatial requirements for site monitoring.

Lateral pressure gradients in the reservoir have the potential to spill trapped CO_2 from a containing trap. This could either be an unwanted side-effect of producing water for some other purpose (see the Volve example below), or of a naturally occurring hydraulic gradient (groundwater flow). Hydraulic gradients and their impact on hydrocarbon-water contacts were first modelled by Hubbert (1953). Specific sites in the North Sea were later analysed (Dennis et al. 2000; 2005) with hydraulic gradients arising from overpressure in the Central Graben. The amount of tilt on a free-water level is directly related to the density difference between the two fluids. At reservoir conditions the density of CO_2 is similar to that of oil and therefore similar amounts of tilt are possible for naturally occurring hydraulic gradients in CO_2 storage reservoirs (Heinemann et al., 2016).

The simulations described below are designed to investigate the interaction of hydraulic gradients and topseal topography by assessing the effect of lateral pressure gradients on the stability of CO_2 buoyantly trapped in small structural closures.

3.1. Model description and parameters

The model extends 11 x 3 km laterally and is 200 m thick with the top located 1000 m below sea-level. A uniform grid is used with a 30 m grid dimension laterally and cell heights increasing from 0.7 m at the top to 20 m at the base, giving a total of 146250 cells. A circular structural dome is positioned at the centre of the domain, 250 m in radius, with a range of model scenarios including dome heights of 1, 2, 5, 10 and 20 m (Figure 10). This corresponds to the type of top reservoir topography encountered by the migrating topmost CO_2 layer at Sleipner (Lindeberg et al. 2001). The dome is initially approximately half-filled with CO_2, the total amount of CO_2 being dependent on the size of the dome (Table 2), with an initialisation simulation ensuring equilibrium of the initial conditions.

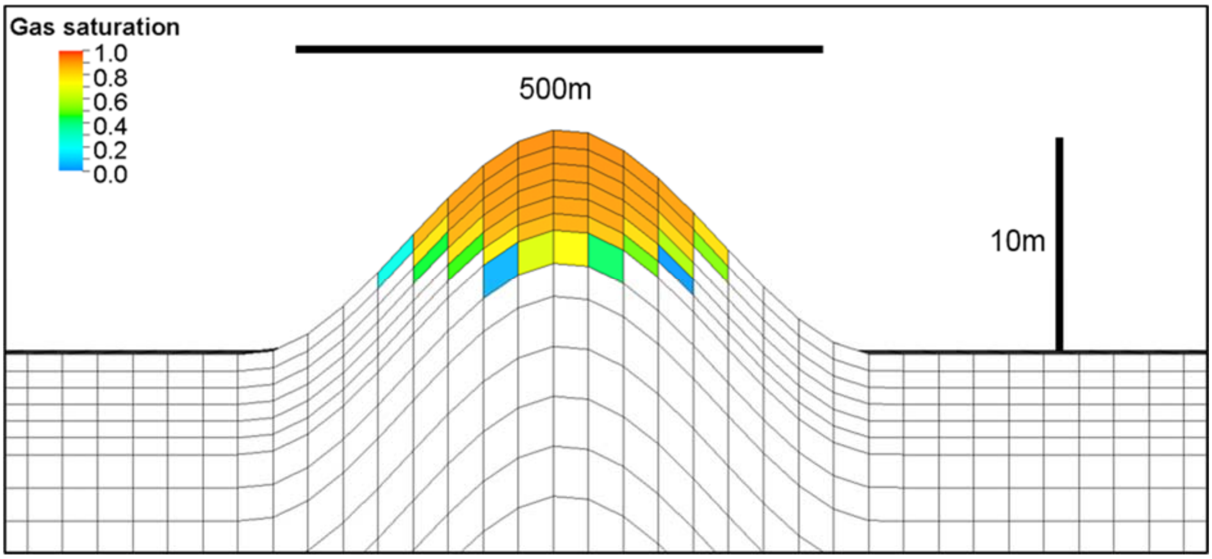

Figure 10: A cross-section through part of the model around the dome (10 m high scenario), half-filled with CO_2 at the initial conditions. 20x vertical exaggeration.

Dome height	1 m	2 m	5 m	10 m	20 m
Total initial mass of free CO_2 (kt)	15.20	19.11	31.51	39.02	99.27
Total initial free CO_2 (x10^3 rm^3)	21.19	26.65	43.95	54.42	138.45

Table 2: Total amounts of free CO_2 initially emplaced in the 10 m structural dome, in units of mass and reservoir volume under average reservoir conditions.

In terms of setting up the hydraulic gradient, a single production well does not really suffice, because its pressure gradient decreases asymptotically from the well (Figure 5). Here we set up an analytically more useful pressure distribution of an approximately linear gradient in one dimension. This is achieved by establishing a two-well water injection-production dipole (Figure 11), with the dome containing CO_2 situated mid-way between the water wells, 5 km from each. Closed boundaries are used in this model to maintain the pressure gradient without transverse leakage.

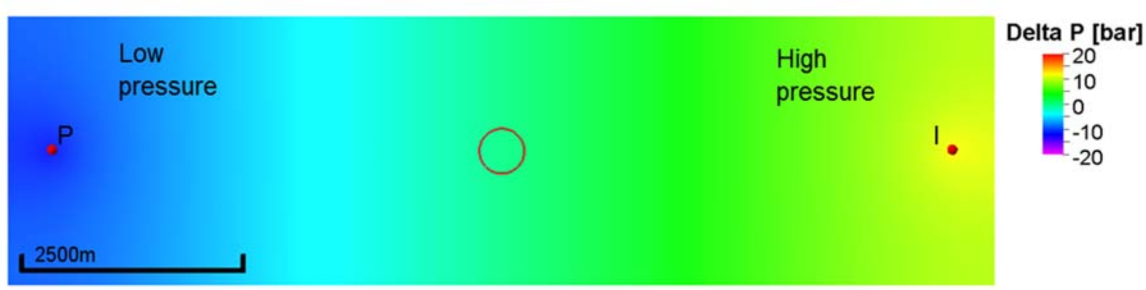

Figure 11: The pressure dipole formed by producing 15 Mt/year of water from the well P and injecting 15 Mt/year of water into the well I. A structural dome where CO_2 is located has its zero-relief spill-point marked by a red circle (250m radius). Delta P is the increase above hydrostatic pressure.

For each of the simulation cases the dome is initially half-full of CO_2 and water circulation is simulated for 20 years. A stable pressure gradient, constant in time, is quickly established after initiation of the water production/injection dipole. After four months of simulation the pressure reaches a steady state and is constant throughout the depth of the model relative to initial hydrostatic values (Figure 11). The established hydraulic gradient is directly related to the rate of water cycling (Table 3), and can approach 2 bar/km for the 15 Mt/year cycling rate. Dennis et al. (2000) report typical hydraulic gradients of 0.35 bar/km in the North Sea, increasing up to 3 bar/km for specific fields such as the Pierce Field. The gradient is linear E-W, except for locally around the wells and within the CO_2 plume, and acts to spill the CO_2 from the dome laterally towards the west.

Water cycling (production/injection) rate	Hydraulic pressure gradient
1 Mt/year	0.13 bar/km
5 Mt/year	0.64 bar/km
10 Mt/year	1.28 bar/km
15 Mt/year	1.92 bar/km

Table 3: Conversion between water injection/production rate and hydraulic pressure gradient.

For comparison with the open aquifer configuration in section 2, an extraction ratio of 1:1 produced 1.42 Mt/year of water.

3.2. Model results

The effect of the imposed pressure gradients is to draw the free CO_2 westwards out of the dome, through its spill-point, towards the low pressure sink (Figures 12 and 13). The amount of CO_2 spilling is a function of the pressure gradient and the dome elevation (Figure 14). It is noted that no CO_2 reaches the production well (5 km west of the dome) in any of the cases simulated. Dissolution continues to occur throughout the simulations, decreasing the amount of free CO_2 in the model as time progresses.

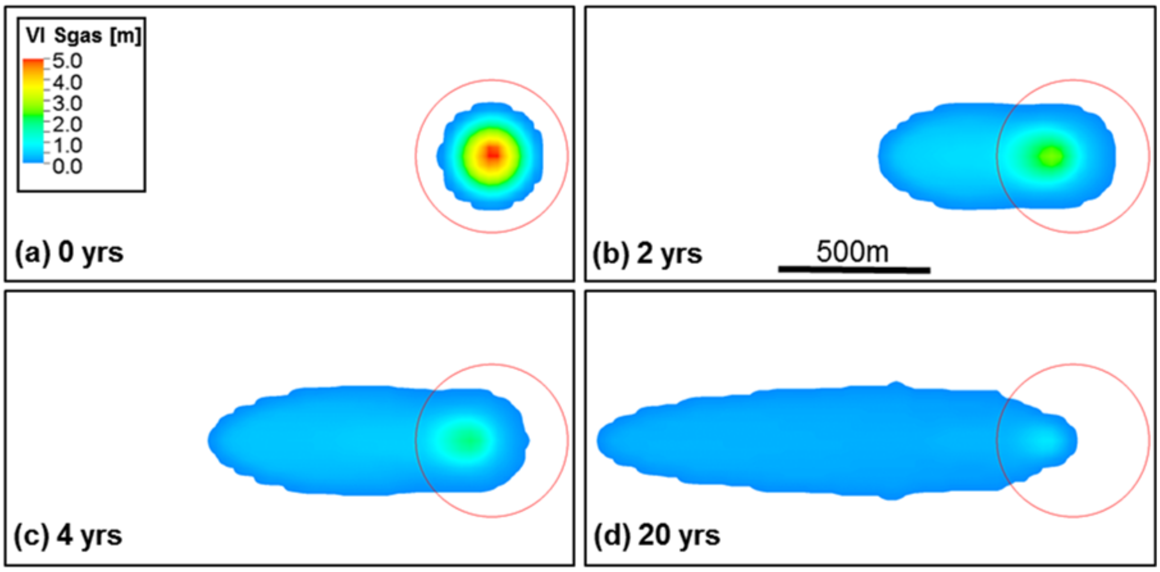

Figure 12: Vertically integrated CO_2 saturation (units in metres, i.e. the total thickness of the CO_2 in the reservoir; to calculate the net CO_2 thickness multiply by the porosity) with a dome height of 10 m and water cycling rate of 10 Mt/year. The dome spill-point (zero-relief contour) shown in red.

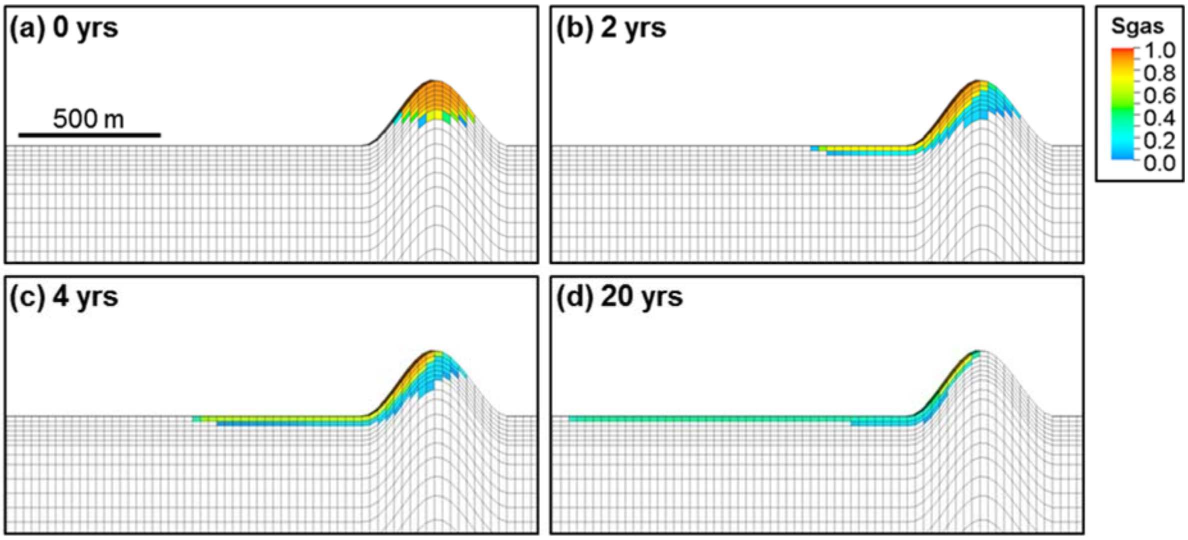

Figure 13: An E-W cross-section of the free CO_2 saturation through the centre of a dome 10 m high with water cycling rate 10 Mt/year at labelled time steps, 25x vertical exaggeration.

The quantities of interest in terms of storage security are the amount of free CO_2 remaining within the dome (inside the 250 m radius zero-relief contour) relative to the initial total, the farthest distance travelled by free CO_2 and the proportion of CO_2 dissolving into the formation water. The latter process is important because dissolved CO_2 is not buoyant and so it markedly increases security of storage.

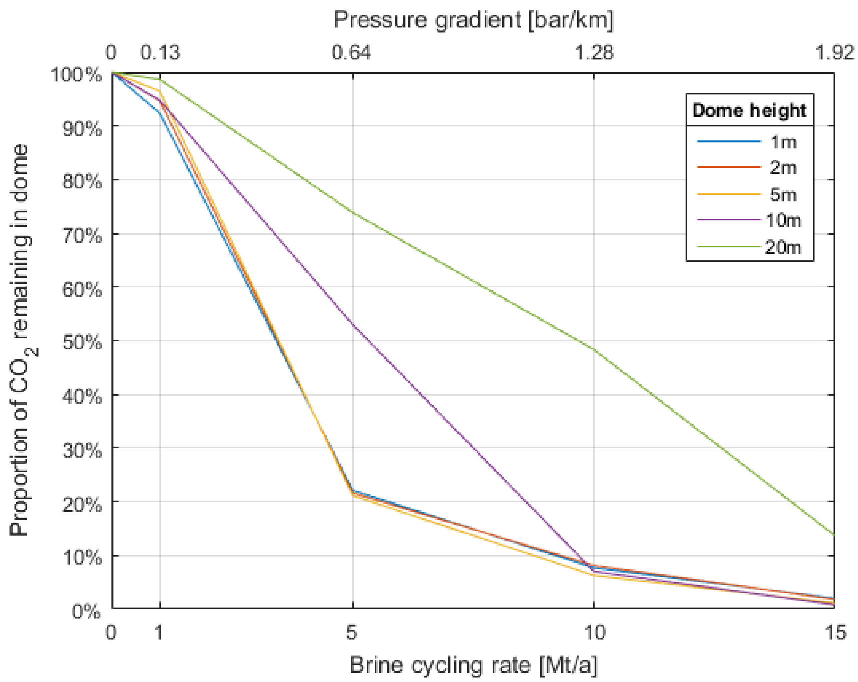

Figure 14: Proportion of CO_2 (free and dissolved) remaining in the dome after 20 years relative to the initial values (Table 1) against injection/production rate for domes heights 1, 2, 5, 10 and 20m.

Both free and dissolved CO_2 is removed from the structural dome as a result of the imposed pressure gradients. A water cycling rate of 1 Mt/year over a period of 20 years spills ~7% of the CO_2 from the 1 m dome, but only ~1% of the CO_2 from the 20 m dome (Figure 14). A significant proportion of CO_2 is spilled when the water cycling rate is increased to 5 Mt/year, especially from the smaller domes. Little difference in the proportion of spilled CO_2 is seen between dome heights of 1 to 5 m, but taller domes require a larger pressure gradient to spill CO_2 because of the larger depth difference between the initial CO_2-water contact (CWC) and the spill-point. Cycling rates of 10 Mt/year and above are sufficient to remove most of the CO_2 from all dome heights over a 20 year period (Figure 14).

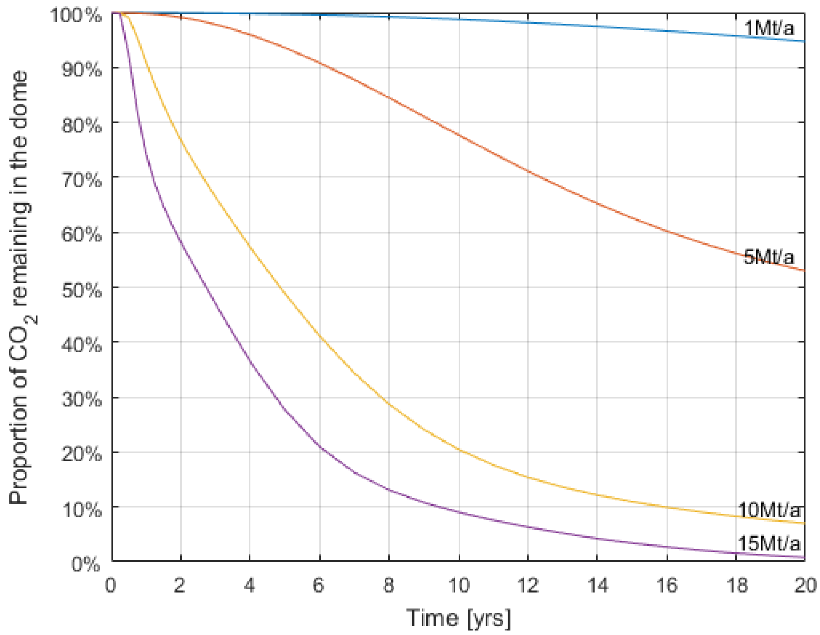

Figure 15: Transient proportion of CO_2 (free and dissolved) remaining within a 10 m dome for a series of water cycling rates (labelled).

The rate at which CO_2 is spilled from a structural trap depends on the size of the dome and the water cycling rate, with for a given dome height, higher cycling rates leading to faster spillage (Figure 15). For 10 Mt/year of water cycling around half of the CO_2 is removed from a 10 m dome after only 5 years. Although this corresponds to a large-scale water management operation, the 5 year time-scale is relatively short, indicative of rapid plume response.

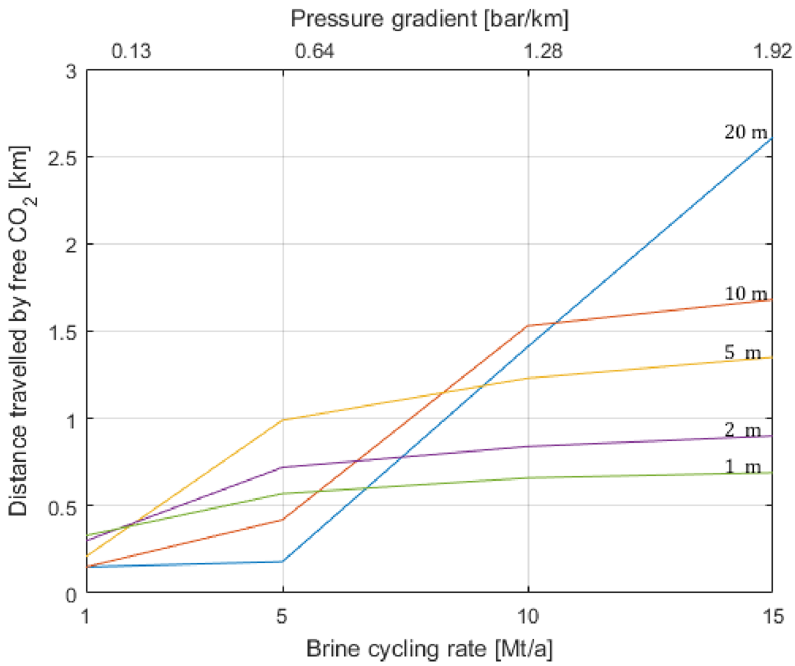

Figure 16: Graph of maximum distance travelled by free (not dissolved) CO_2 measured from the centre of the dome (250 m radius) after 20 years against water cycling rate for different dome heights (labelled).

The distance migrated by free CO_2 is a good indicator of plume steering potential. For cycling rates of 1 – 2 Mt/year, free CO_2 is not transported past the spill-point of any of the domes more than 2 m high (Figure 16). Cycling rates of 5 Mt/year produce some spillage from domes up to 10 m tall but do not tilt the CWC sufficiently (through 10 m of depth change) to spill any CO_2 from the 20 m dome. It is notable that higher cycling rates (>5 Mt/year) do not produce a proportionate increase in migration distance for the 1 m and 2 m domes. This is because the amount of free CO_2 initially available is quite small (Table 2) and dissolution removes most of this as it migrates laterally (see below). For the taller domes more CO_2 is available, so provided the pressure gradient is sufficient to bring it to the spill-point, then the free CO_2 plume will travel further overall before dissolution reduces its size. Provided that the amount of CO_2 is not a limiting factor then the distance travelled is proportional to the pressure gradient – as evidenced by the 20 m dome scenario (Figure 16).

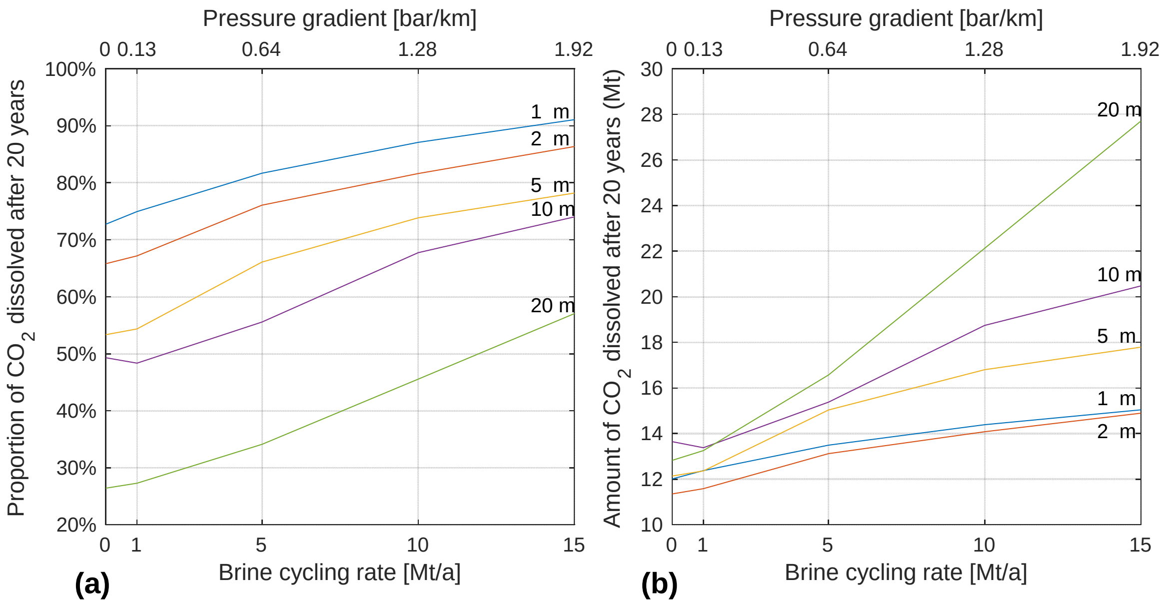

Figure 17: CO_2 dissolution after 20 years plotted against water cycling rate for different dome sizes (labelled). (a) Proportion relative to the amount of CO_2 initially emplaced (b) absolute amount of CO_2.

The amount of CO_2 dissolving in the different cases can be measured either as a proportion of the total CO_2 initially within the dome or as an absolute quantity (Figure 17). It is clear that water cycling strongly enhances CO_2 dissolution, although for the smallest dome (1 m tall), most of the CO_2 (~73%) dissolves into the water even without water cycling. This is due to the relatively large spatial area of theCO_2-water contact compared with the small amount of emplaced free CO_2. The more general tendency for water cycling to increase dissolution has two causes. Firstly water-cycling increases the plume footprint through spillage and so more free CO_2 is in contact with the surrounding reservoir water. This is most notable for the 20 m dome where a relatively large migrating plume is susceptible to dissolution (Figure 17b). A second, more subtle effect is also evident. If we consider the 20 m dome, for cycling rates up to around 5 Mt/year, no CO_2 is spilled from the dome and there is no increase in its spatial footprint (Figure 16). Dissolution nevertheless increases from around 26% with no cycling to ~34% with cycling at 5 Mt/year (Figure 17). This is because with no cycling a boundary layer of CO_2-saturated water forms beneath the CWC and further dissolution is limited by diffusion across the boundary layer. With water cycling, CO_2-saturated water beneath the CWC is continuously swept away to be replaced by CO_2-free water; this allows for much more rapid diffusion and dissolution at the constantly renewed CO_2-water interface.

To conclude, a cycle rate of 5 Mt/year was found sufficient to spill a significant amount (>30%) of CO_2 trapped in domes up to 20 m tall. A sustained pressure gradient of sufficient magnitude was shown to continuously spill CO_2 from a structural trap and, albeit with an idealised flat topseal, to generate a mobile plume migrating more than 2.5 km in 20 years. Increasing the sweep of a CO_2 plume by removing it from a structural trap increases the potential for dissolution and residual trapping.

4. Sleipner and Volve

At the Sleipner CO_2 storage project (Baklid et al. 1996), CO_2 is being stored in the Utsira Sand, a large saline aquifer in the Norwegian sector of the North Sea. A multi-layered plume of CO_2 has accumulated in the reservoir since injection commenced in 1996 (e.g. Chadwick et al., 2009, Williams and Chadwick, 2017). The topmost layer of CO_2 in the plume is pooling directly beneath the mudstone topseal and migrating generally towards the north. Time-lapse seismic data show that the CO_2 in this topmost layer is migrating buoyantly via a fill-spill mechanism within small topographic domes and ridges in the topseal, whose relief ranges from just a few metres up to about 20 m (Figure 18).

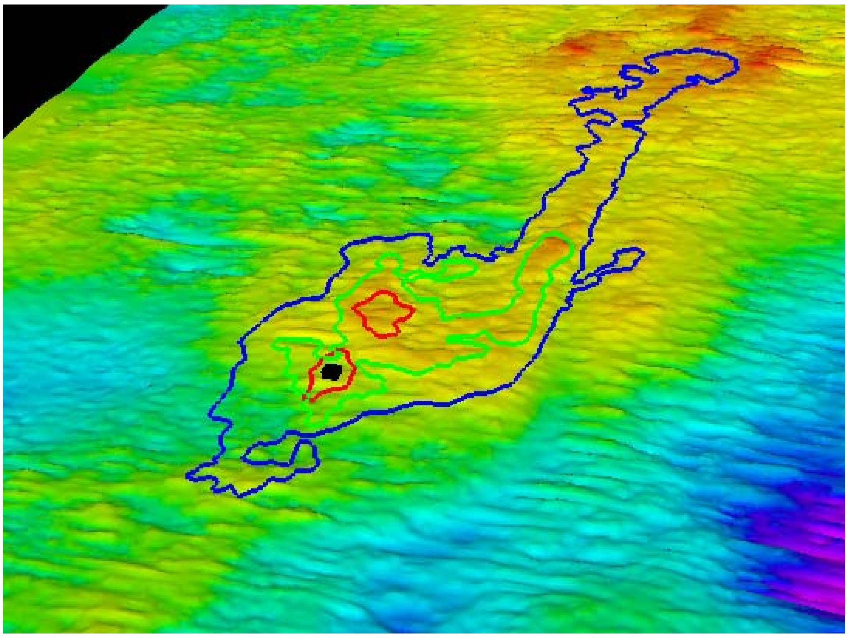

Figure 18: Perspective view (looking north) of the top of the Utsira Sand reservoir at Sleipner showing mapped extents from time-lapse seismics of the topmost CO_2 layer in 1999 (red), 2001 (green) and 2006 (blue). Note the prominent north-trending linear ridge demarcated by the layer extents in 2006. Distance from the southern tip of the 2006 polygon to the northern tip is about 3 km. The black marker denotes the position of the principle feeder of CO_2 from the deeper plume.

An additional model scenario applies the principles of our theoretical study to the Sleipner CO_2 storage operation and nearby water production at the Volve oil field, some 8 km to the northwest. Injection of CO_2 at Sleipner is ongoing since 1996 and Volve was operational as an oil field from 2008 to 2016. At the peak of production in 2009 Volve produced 3.16 million sm^3 oil per year (including small amounts of condensate, NGL and gas, source: Norsk Petroleum). Water was produced from the Utsira Sand and reinjected into the much deeper oil reservoir to provide pressure support for oil recovery. From 2009 to 2015 water production rates were roughly between 1.9 and 3 M sm^3/year (Norwegian Petroleum Directorate).

To simulate this situation, a numerical model was built with a dome measuring 500 m in diameter and 10 m high containing CO_2 to the spill-point, together with a water production well positioned 8 km from the dome centre. The model dimensions are 10 km x 3 km with 30 m grid resolution and 200 m reservoir thickness with layering identical to the previous two models in this study. Quasi-infinite pore volume multipliers are applied to the edges of the model to simulate open boundaries with the large surrounding aquifer, consistent with the properties of the Utsira Sand (Chadwick et al. 2012). The model top is set at a depth of 1000 m to approximate the Sleipner reservoir pressure and temperature conditions.

Water is produced at a rate of 3.2 Mt/year, equivalent to 3 M sm^3/year, the higher end of the reported water production range and continues for 40 years. This high value of water production is chosen to give an indication of the maximum impact production at Volve might have on the CO_2 at Sleipner. Close to the production well the induced pressure gradient exceeds 1.5 bar/km, but this reduces to only ~$6x10^{-5}$ bar/km in the vicinity of the CO_2 plume. This is much smaller than the hydraulic gradients modelled above (Table 3), and no effect was discernible on modelled CO_2 fluid distributions. For comparison with the open aquifer model, 3.2 Mt/year is equivalent to an extraction ratio of 2.2:1, although in this case the production well is located further away and production continued for a longer time. A second simulation was run with a water production rate of 32 Mt/year (ten times the amounts at Volve). This produces a pressure gradient of 15 bar/km around the production well, and ~$6x10^{-4}$ bar/km at the CO_2 plume, but still no difference in CO_2 distribution is noted, with no detectable lateral spillage from the dome, despite it being filled to the spill-point.

We conclude that production from the Volve water production operation is too small and far away to have any detectable effect on the position and migration of the CO_2 plume at Sleipner. This result is supported by the time-lapse 3D seismic data which indicate that in the more distal parts of the topmost layer, CO_2 migration beneath the topseal is governed only by buoyancy-driven migration (Chadwick and Noy, 2010).

5. Concluding remarks

The effectiveness of water production for influencing the trajectory of a migrating CO_2 plume depends on wider-scale water flow in the reservoir. The pressure gradient of water production from a single modelled well tends to propagate radially and so has a greater impact when channelled in a single direction, such as by flow boundaries. In open homogeneous aquifers the influence of water production can spread over a wide area and even water production rates up to 10 times the volume of injected CO_2 have a very limited impact on a plume only 5 km away, particularly if the natural path of buoyant CO_2 is not altered by the breaching of topographical spill-points. Impact is also limited by the permeability of the reservoir, given realistic time durations for water production.

In compartmentalised reservoirs, water production can have a noticeable impact. Cycling 5 Mt/year of water through a water production-injection dipole in a model with closed boundaries had a larger impact on CO_2 migration than producing 10 Mt/year from an open aquifer through a single well. This is because in an open aquifer the surrounding pore space provides recharge for the reservoir, neutralising the pressure sink created by water production. Our simulations with a closed aquifer and water cycling rates of 15 Mt/year showed CO_2 migration distances of up to 2.5 km over a 20-year period.

Turning to the possible effects on CO_2 storage at Sleipner of water production at the nearby Volve field, our calculations indicate that in the large, open, Utsira Sand aquifer, the water production is too far from the plume to noticeably influence the migration of CO_2. Only very small hydraulic pressure gradients are induced in the vicinity of the Sleipner plume, insufficient to move CO_2 out of currently occupied topographic traps. This is supported by the time-lapse seismic monitoring results.

More generally, the well dipole closed-boundary models showed that induced hydraulic gradients in the range 1 – 2 bar/km are capable of drawing CO_2 laterally out of small topographic traps. These values are in the range of natural head gradients that would result from a reservoir topographic relief of 1000 metres dissipated over a distance of 50 to 100 km. Lateral pressure gradients of this order are not uncommon (e.g. Dennis et al., 2000), so it is clear that CO_2 migration modelling should take into account natural groundwater flows wherever these are likely to be significant, notably in onshore basins with significant relief. Conversely, in situations such as at Sleipner, where there is no hydraulic gradient from a connected onshore aquifer, any 'plume steering' effects due to natural water flow can probably be disregarded.

Many of our simulations involved producing a greater volume of water than the volume of CO_2 injected with a consequent net fluid/pressure depletion of the site. This might have implications for neighbouring storage sites, connected hydrocarbon fields, mechanical integrity of the reservoir and caprock and, ultimately, the economics of the water production operation.

The studies utilised simplified reservoir models with homogeneous properties. The impact of water production will be further complicated by smaller-scale permeability heterogeneity, affecting both the shape as well as the extent of the plume. To apply these principles to a specific storage site would require more detailed modelling incorporating an appropriately detailed level of heterogeneity.

The work presented here has the potential to be taken forward in a more generalised analysis, for example by determining a 'critical' value of hydraulic gradient necessary for effective plume steering. There are complexities to this however, in particular reservoir permeability would inversely scale the critical hydraulic gradient, and so generalisation involving the development of a critical gradient - permeability parameter might be the best way forward. Buoyancy of the free CO_2 plume will also have an effect and it might be instructive to compare the relative effects of hydraulic gradient with plume buoyancy forces for different topseal dips.

Acknowledgements

This paper was prepared as part of the research project 'CO_2 Injection and Storage – Short and long-term behaviour at different spatial scales' (EPSRC Grant: EP/K035967/1), with additional support from the UKCCS Research Centre (EPSRC Grant EP/P026214/1). Thanks also to Schlumberger for the use of PETREL and ECLIPSE software. The authors publish with the permission of the Executive Director, BGS (NERC).

References

Baklid, A., Korbøl, R., Owren, G., 1996. Sleipner Vest CO_2 disposal, CO_2 injection into a shallow underground aquifer. SPE paper 36600. SPE Annu. Tech. Conf. Exhib., Denver, CO, USA, 6-9 Oct 1996.

Bergmo, P.E., Grimstad, A.A., Lindeberg, E., 2011. Simultaneous CO_2 injection and water production to optimise aquifer storage capacity. Int. J. Greenh. Gas Control 5, 555–564.

Birkholzer, J.T., Cihan, A., Zhou, Q., 2012. Impact-driven pressure management via targeted water extraction: Conceptual studies of CO2 storage in saline formations. Int. J. Greenh. Gas Control 7, 168–180.

Breunig, H. M., Birkholzer, J. T., Borgia, A., Oldenburg, C. M., Price, P. N., and McKone, T E. 2013. Regional evaluation of brine management for geologic carbon sequestration. Int. J. Greenh. Gas Control 14, 39-48.

Buscheck, T.A., Sun, Y., Chen, M., Hao, Y., Wolery, T.J., Bourcier, W.L., Court, B., Celia, M.A., Julio Friedmann, S., Aines, R.D., 2012. Active CO_2 reservoir management for carbon storage: Analysis of operational strategies to relieve pressure buildup and improve injectivity. Int. J. Greenh. Gas Control 6, 230–245.

Buscheck, T.A., Sun, Y., Hao, Y., Wolery, T.J., Bourcier, W., Tompson, A.F.B., Jones, E.D., Julio Friedmann, S., Aines, R.D., 2011. Combining water extraction, desalination, and residual-water reinjection with CO_2 storage in saline formations: Implications for pressure management, capacity, and risk mitigation. Energy Procedia 4, 4283–4290. doi: 10.1016/j.egypro.2011.02.378

Cameron, D.A., Durlofsky, L.J., 2012. Optimization of well placement, CO_2 injection rates, and water cycling for geological carbon sequestration. Int. J. Greenh. Gas Control 10, 100–112. doi: 10.1016/j.ijggc.2012.06.003

Chadwick, R.A., Noy, D.J., 2010. History-matching flow simulations and time-lapse seismic data from the Sleipner CO_2 plume, in: Petroleum Geology Conference Series. pp. 1171–1182.

Chadwick, R.A., Noy, D., Arts, R., Eiken, O., 2009. Latest time-lapse seismic data from Sleipner yield new insights into CO_2 plume development. Energy Procedia 1, 2103–2110.

Chadwick, R. A., Noy, D. J., Holloway, S. 2009. Flow processes and pressure evolution in aquifers during the injection of supercritical CO_2 as a greenhouse gas mitigation measure. Petroleum Geoscience 15, 59-73.

Chadwick, R.A., Williams, G.A., Williams, J.D.O., Noy, D.J., 2012. Measuring pressure performance of a large saline aquifer during industrial-scale CO_2 injection: The Utsira Sand, Norwegian North Sea. Int. J. Greenh. Gas Control 10, 374–388.

Cihan, A., Birkholzer, J. T., Bianchi, M. 2015. Optimal well placement and brine extraction for pressure management during CO_2 sequestration. Int. J. Greenh. Gas Control 42, 175-187.

Court, B., Bandilla, K.W., Celia, M.A., Buscheck, T.A., Nordbotten, J.M., Dobossy, M., Janzen, A., 2012. Initial evaluation of advantageous synergies associated with simultaneous water production and CO_2 geological sequestration. Int. J. Greenh. Gas Control 8, 90–100. doi: 10.1016/j.ijggc.2011.12.009

Court, B., Celia, M.A., 2011. Safety and water challenges in CCS: Modeling studies to quantify CO_2 and water leakage risk and evaluate promising synergies for active and integrated water management. Civ. Environ. Eng. Princeton University.

Dennis, H., Baillie, J., Holt, T., Wessel-Berg, D. 2000. Hydrodynamic activity and tilted oil-water contacts in the North Sea. 171-185 in Improving the Exploration Process by Learning from the Past. Ofstad, K, Kittilsen, J E, and Alexander-Marrack, P (editors). NPF Special Publication 9. (Amsterdam: Elsevier Science B. V.)

Dennis, H., Bergmo, P., Holt, T. 2005. Tilted oil-water contacts: Modelling the effects of aquifer heterogeneity. Geological Society, London, Petroleum Geology Conference series, 6, 145-158.

Heinemann, N., Stewart, R. J., Wilkinson, M., Pickup, G., Haszeldine, R. S. 2016. Hydrodynamics in subsurface CO_2 storage: Tilted contacts and increased storage security. Int. J. Greenh. Gas Control 54, 322-329.

Hubbert, M. K. 1953. Entrapment of petroleum under hydrodynamic conditions. Bulletin of the American Association of Petroleum Geologists, Vol. 37, 1954-2026.

Le Guenan, T., Rohmer, J., 2011. Corrective measures based on pressure control strategies for CO_2 geological storage in deep aquifers. Int. J. Greenh. Gas Control 5, 571–578.

Leonenko, Y., Keith, D.W., 2008. Reservoir engineering to accelerate the dissolution of CO_2 stored in aquifers. Environ. Sci. Technol. 42, 2742–2747. doi: 10.1021/es071578c.

Lindeberg, E., Zweigel, P., Bergmo, P., Ghaderi, A., Lothe, A. 2001. Prediction of CO_2 distribution pattern improved by geology and reservoir simulation and verified by time-lapse seismic. . In: Williams, D., Durie, I., Mcmullan, P., Paulson, C. & Smith, A. (eds.). Greenhouse Gas Control Technologies. Proceedings of the 5th International Conference on Greenhouse Gas Control Technologies. CSIRO Publishing, 372 – 377.

NIST, 2016. Thermophysical Properties of Fluid Systems http://webbook.nist.gov/chemistry/fluid/. [cited 04/08/2015].

Norsk Petroleum. http://www.norskpetroleum.no/fakta/felt/volve/. [cited 2 Feb 2017].

Norwegian Petroleum Directorate. http://factpages.npd.no/factpages/. [cited 27 Apr 2017].

Noy, D.J., Holloway, S., Chadwick, R.A., Williams, J.D.O., Hannis, S.A., Lahann, R.W., 2012. Modelling large-scale carbon dioxide injection into the Bunter Sandstone in the UK Southern North Sea. Int. J. Greenh. Gas Control 9, 220–233.

Vella, D., Huppert, H.E., 2006. Gravity currents in a Porous medium at an inclined plane. J. Fluid Mech. 555, 353–362. doi:10.1017/S0022112006009578

Williams, G.A., Chadwick, R.A., 2017. An improved history-match for layer spreading within the Sleipner plume including thermal propagation effects. Energy Procedia, 114, 2856-2870.